Applied Surface Science 505 (2020) 144512

Contents lists available at ScienceDirect

Applied Surface Science

journal homepage: www.elsevier.com/locate/apsusc

Full Length Article

Toward enhanced CO_2 adsorption on bimodal calcium-based materials with porous truncated architectures

Soonchul Kwon[a,b,1], Hyuk Jae Kwon[a,1], Ji Il Choi[c], Hyun Chul Lee[a,*], Armistead G. Russell[d], Seung Geol Lee[e], Taeyoon Kim[b], Seung Soon Jang[c,*]

[a] Samsung Particulate Matter Research Institute, Samsung Advanced Institute of Technology (SAIT), Samsung Electronics Co., LTD, 130 Samsung-ro, Yeongtong-gu, Suwon-si, Gyeonggi-do 16678, Republic of Korea
[b] Department of Civil and Environmental Engineering, Pusan National University, 2, Busandaehak-ro 63beon-gil, Geumjeong-gu, Busan 46241, Republic of Korea
[c] School of Materials Science and Engineering, Georgia Institute of Technology, Atlanta, GA 30332-0245, USA
[d] School of Civil and Environmental Engineering, Georgia Institute of Technology, Atlanta, GA 30332-0355, USA
[e] Department of Organic Materials Science and Engineering, Pusan National University, 2 Busandaehak-ro, 63beon-gil, Geumjeong-gu, Busan 46241, Republic of Korea

ARTICLE INFO

Keywords:
Carbon dioxide
Adsorption
Calcium oxide
Density functional theory
Porous structure

ABSTRACT

To increase the mineralization capabilities for the adsorption of carbon dioxide, we prepared bimodal calcium-based materials such as calcium oxide and calcium hydroxide with porous structures using a precipitation method with various drying processes. The various drying methods on porous structure develop different composition ratio of CaO and $Ca(OH)_2$ in bimodal materials, and in particular, formation of different morphology and structure, which leads different adsorption characteristics. Samples prepared with such methods attained porous structure and more active adsorption sites. It is worth noting that the freeze drying (FD) and aerogel drying (AD) methods created the truncated crystal phase of the adsorbents, exposing active facet sites in the place of the vertices. The results of CO_2 temperature programmed desorption and dynamic flow experiments reveal that porous calcium-based materials, synthesized through a process combining FD and AD sequentially, show high CO_2 adsorption capacity (up to 26.1 wt% at 650 °C) with enhanced adsorption kinetics. To gain insight into CO_2 adsorptive configuration at the atomistic scale and the adsorption mechanism, the adsorption of multiple CO_2 molecules on the CaO (1 0 0) surface is investigated using density functional theory calculation. The CO_2 molecules are chemisorbed through active charge reorganization between the CaO surface and CO_2 molecules while the adsorption energy is highly stabilized at –1.56 eV. The experimental and theoretical findings both suggest that CO_2 mineralization is feasible on calcium-based bimodal structured materials.

1. Introduction

In recent times, significant climatic changes have been observed globally owing to increased greenhouse gas emissions into the atmosphere. Carbon dioxide accounts for 94% of the total greenhouse emissions in the world, with over 80% of the anthropogenic CO_2 emissions generated through energy production [1]. Thus, in order to combat climate change, researchers have focused on reducing CO_2 emissions from power generation facilities. These facilities produce flue gas mixtures, which constitute the largest anthropogenic emission source of CO_2, accounting for ~41% of the total CO_2 emissions [2,3]. Therefore, many separation technologies have been developed and are widely used for CO_2 sequestration [4–13].

Among various CO_2 separation processes, the usage of solid state sorbents such as minerals for CO_2 adsorption has been intensively studied owing to benefits such as low operating cost, low energy demand, stable recycling capacity, and high CO_2 selectivity [14–17]. In addition, solid state sorbents are relatively easy to handle compared to liquid sorbents [18,19], since the former present less corrosion problems than the latter. For CO_2 sequestration, mineral carbonation using alkaline-earth metal oxides such as calcium oxide (CaO) and hydrated lime ($Ca(OH)_2$) appears to be particularly promising because the metal oxides react with CO_2 to form stable carbonates, which exhibit very low CO_2 leakage after sequestration [11,20–22]. Furthermore, the stable carbonates produced from this carbonation process could be treated through environmentally friendly processes such as mine reclamation and soil amendment [11].

In the gas-solid carbonation process, the alkaline-earth metal oxides

* Corresponding authors.
E-mail addresses: hc001.lee@samsung.com (H.C. Lee), seungsoon.jang@mse.gatech.edu (S.S. Jang).
[1] Soonchul Kwon and Hyuk Jae Kwon equally contributed to the work.

https://doi.org/10.1016/j.apsusc.2019.144512
Received 25 June 2019; Received in revised form 24 October 2019; Accepted 25 October 2019
Available online 05 November 2019
0169-4332/

react exothermically with CO_2, where the basicity of the metal oxides determines the reactivity with respect to CO_2 [23]. For example, CO_2 molecules bind to the oxygen atoms on the CaO surface to form calcium carbonate ($CaCO_3$), and on the $Ca(OH)_2$ surface to form carbonate and water vapor. The gas-solid carbonation of calcium-based adsorbents can be expressed by the following global chemical reactions in Eqs. (1) and (2):

$$CaO(s) + CO_2(g) \rightarrow CaCO_3(s), \quad \Delta H_{CO2} = -178.15\ kJ/mol \tag{1}$$

$$Ca(OH_2)(s) + CO_2(g) \rightarrow CaCO_3(s) + H_2O(g), \quad \Delta H_{CO2} = -69.02\ kJ/mol \tag{2}$$

This gas-solid carbonation processes using alkaline sorbents have their potential to capture CO_2 via non-catalytic exothermic reactions, allowing the selective mineralization of CO_2 from a gas mixture. This carbonation occurs via charge transfer from the CaO or $Ca(OH)_2$ surface to CO_2 molecule [24]. The theoretical amount of CO_2 adsorbed on CaO and $Ca(OH)_2$ is 17.8 mmol/g_{Cao} and 13.5 mmol/$g_{cao(OH)}$, relatively, whereas the actual amount is relatively lower (< 4.5 mmol/g_{Cao} and < 11 mmol/$g_{cao(OH)}$, relatively), due to the limited reaction kinetics [25]. Thus, it still has a margin to improve the CO_2 uptake by modifying the material properties. In particular, we can expect the synergic effect of $Ca(OH)_2$ on CaO carbonation, owing to the relatively high activity of hydrated phase.

In addition to the inherently high affinity of adsorbent towards CO_2, porous crystal adsorbents would be even more beneficial in enhancing the CO_2 capture capacity, because more active sites would be exposed in porous structure. Along this line, various structures of adsorbents with varying compositions have been synthesized to improve the adsorption capacity of CaO as well as long–term cyclic performance. Hughes et al. [26] and Sun et al. [27] also reported that the hydration of pre-calcined calcium-based adsorbents enhanced their CO_2 adsorption performance. Thus, we have examined the effect of the bimodal structure of calcium-based materials composed of calcium oxide and hydrated calcium materials on promoting CO_2 adsorption.

In this study, we attempt to develop porous bimodal calcium-based materials composed of CaO and $Ca(OH)_2$, using a precipitation method without a template. In order to improve affinity towards CO_2, various drying processes such as conventional oven drying (OD), freeze drying using liquid N_2 (FD), and aerogel drying using supercritical fluid CO_2 (AD) have been applied for modifying the morphology and structure of the prepared samples. In particular, a combination of drying processes involving FD and AD (FAD) was applied to generate larger active sites for CO_2 uptake. The desired structures attain a large amount of pore with more adsorption sites, improving CO_2 uptake affinity. In addition, the bimodal structure controlled by relative amounts of CaO and Ca$(OH)_2$ has a unique truncated phase to expose new active facet sites. The porous truncated structure and its effect on the structural stability and surface chemistry of the adsorbent were verified with both static adsorption experiment using CO_2 temperature programed desorption (TPD) profile and dynamic adsorption experiment using flue CO_2 gas stream mixture. In addition, we carried out cycling performances to determine the improved durability of the synthesized materials.

Furthermore, we have also investigated CO_2 adsorption on a mineral oxide surface, specifically CaO (1 0 0) surface using the density functional theory (DFT) to achieve a fundamental understanding of CO_2 adsorption on the synthesized adsorbent at the molecular level. Since CO_2 chemisorption capacities according to $Ca(OH)_2$ contents shows the asymmetrical "volcano-type" relation under narrow compositional window, which means a limited content of $Ca(OH)_2$ shows the maximum chemisorption capacity, we mainly focused on CaO contents as the bimodal structure for theoretical calculation. Although there are a few theoretical studies on the adsorption of a single CO_2 molecule on a CaO surface [23,28–32], there have been no studies on the adsorption of multiple CO_2 molecules to the extent of our knowledge, which would be critical for assessing the adsorption characteristics of CaO. It is well known that the intermolecular interaction among CO_2 molecules affects the adsorption properties on the metal-oxide surface in the previous study [33–35]. Therefore, we calculated various configurations for multiple CO_2 adsorption on the CaO (1 0 0) surface in an attempt to understand the adsorption mechanism as well as accompanying characteristics such as the most stable number of CO_2 molecules, charge transfer between CO_2 and CaO surface, and surface charge redistribution. Finally, we proposed, based on the findings in this study, a key rule of porous bimodal adsorbent design for high CO_2 uptake.

2. Experimental section

2.1. Synthesis procedure

Seven different types of CaO samples, namely (1) CaO-CV, (2) CaO-OD, (3) CaO-FD, (4) CaO-AD, and (5) CaO-FAD, were synthesized using various procedures. Conventional CaO (CaO-CV) was purchased from Sigma-Aldrich (USA) for use as a reference.

2.1.1. CaO synthesis

CaO was prepared by the calcination of $Ca(OH)_2$ at 550 °C for 5 h in air. For producing porous CaO crystals, initially, 10 wt% of 2 M NaOH solution was slowly added at the rate of 2 mL/min to 10 wt% of 1 M Ca$(NO_3)_2{\cdot}4H_2O$ solution with vigorous stirring. This resulted in the precipitation of Ca-based materials

2.1.2. Preparation of CaO-OD (oven drying)

Precipitation was carried out at 100 °C. The precipitate was aged for 24 h at 25 °C with continuous stirring, following which it was filtered and washed thoroughly with distilled water until the pH of the filtrate was almost neutral (pH < 7.5). The filtered sample was dried in an oven at 120 °C for 12 h and subsequently calcined at 550 °C for 5 h under air flow.

2.1.3. Preparation of CaO-FD (freezing drying)

These samples were prepared using a procedure similar to that used for CaO-OD, except that the samples were freeze dried in this case.

Freezing drying process has been performed at liquid nitrogen. The adsorbents were frozen at −196 °C for about 15 min with liquid nitrogen and then slowly sublimated at room temperature and vacuum condition to keep the original shape of the product without pore shrinkage and high quality of the rehydrated product as much as possible.

2.1.4. Preparation of CaO-AD (aerogel drying)

The samples were prepared similar to CaO-OD up to the drying stage. Subsequently, the samples were dried using aerogel drying (AD) for 3 h. In aerogel drying, the sample was transferred in a supercritical dryer with 100% CO_2 as co-solvent. Then, they were calcined at 550 °C for 5 h and at 900 °C for 5 h in succession.

2.1.5. Preparation of CaO-FAD (Freezing and aerogel drying)

The preparation procedure was similar to that used for CaO-OD, except that the samples were dried by FD for 3 h and AD for 3 h applied sequentially, followed by first calcination at 550 °C for 5 h and next at 900 °C for 5 h in succession.

2.2. Characterizations

The adsorbent samples were characterized using various structural and morphological methods including transmission electronic microscopy (TEM), X-ray diffraction (XRD), and Brunauer-Emmett-Teller (BET) analysis. Bright-field TEM images were obtained using a Tecnai G2 TEM (FEI) operated at 200 kV. The sample was deposited on a Cu grid covered by a holey carbon film for the TEM measurements. The

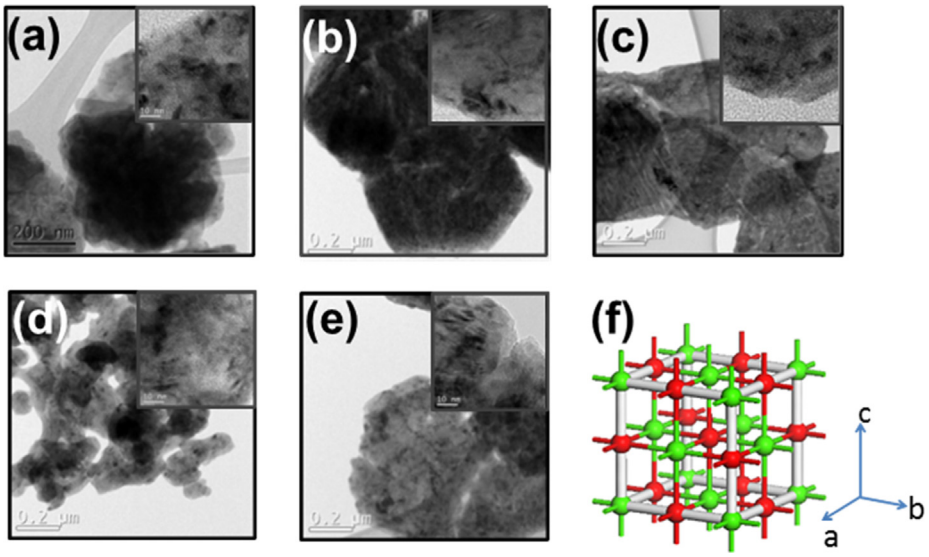

Fig. 1. TEM images of the transformed phase of porous CaO for samples prepared with various drying methods: (a) CaO-CV (conventional CaO), (b) CaO-OD, (c) CaO-FD, (d) CaO-AD, (e) CaO-FAD, and (f) Geometry of the CaO unit structure. The inset figures are at 10 nm resolution.

bulk crystalline structure of the catalysts was determined using the XRD technique. The XRD patterns were obtained using Cu Kα radiation (40 kV) on a Phillips XPert PRO instrument at room temperature. The relative contents of CaO and $Ca(OH)_2$ were calculated by quantitative analysis determining the relative factor through integrated intensity of the XRD peaks with the Rietveld refinement. For determining the BET surface area, N_2 adsorption/desorption isotherm data were obtained at −196 °C using a volumetric apparatus by Bell SorpMax (Bell Japan). The prepared samples were degassed at 200 °C for 24 h before the measurements. Pore size distributions were determined from the adsorption isotherms using the Barrett-Joyner-Halenda (BJH) model with cylindrical pore geometry, and the pore volumes were measured at $P/P_0 > 0.97$. Next, we performed a CO_2-temperature programmed desorption (TPD) experiment to determine the amount of CO_2 chemisorbed on the CaO adsorbent. Micromeritics 2950 chemisorption analyzer was used for these experiments. The samples were pre-treated at 500 °C for 1 h with Ar and CO_2-TPD analysis was carried out in the temperature range of 25–800 °C with a ramp rate of 10 °C/min.

2.3. Computational details

In this study, we employed quantum mechanical DFT, which is a method for evaluating electronic structures and properties of materials. The model was implemented using $DMol^3$ module at Materials studio [33,39]. DFT has been widely used for studying condensed matter systems including surfaces [40–44]. Among various functionals available for DFT, we used the generalized gradient approximation (GGA) Perdew-Burke-Ernzerhof (PBE) functional [45,46] with double numerical basis plus polarization (DNP) basis sets, which have been widely used in the fields of materials science as well as physics [30,47–52]. The DFT calculations were performed at 0 K without pressure and zero-point motion.

The surface of CaO (1 0 0) was constructed based on its crystal structure (Fig. S1) [53] and the atomic positions were refined by performing geometry optimization. The first three layers were geometry-optimized without constraints. The convergence tolerances for energy and SCF density were 2×10^{-5} Ha and 1×10^{-5} Ha, respectively.

The CO_2 adsorption energy ($\Delta E_{adsorption}$) on the CaO (1 0 0) surface was calculated using Eq. (3):

$$\Delta E_{adsorption} = \frac{E_{CaO-CO_2} - (E_{CaO} + n \times E_{CO_2})}{n} \quad (3)$$

where $E_{Cao\text{-}CO2}$ is the energy of the entire system consisting of CO_2 molecules adsorbed on the CaO surface, E_{Cao} and E_{CO2} are the energies of the bare CaO surface without CO_2 and a single CO_2 molecule in vacuum, respectively, and n denotes the number of CO_2 molecules loaded on the CaO surface.

For this study, the (2 × 2) supercell (9.621 Å × 9.621 Å) of the CaO (1 0 0) surface was mainly employed as shown in Fig. S1c, unless specified otherwise. The thickness of vacuum (i.e., size of the unit cell perpendicular to the slab-slab thickness) was fixed at 30 Å for all the calculations. The dimension of the initial computational cell was 9.621 Å × 9.621 Å × 37.216 Å. In order to analyze the electronic effect of k-point sampling on the structure and energy of the system, various k-point samplings for the Brillouin zone were implemented using the Monkhorst-Pack k-point scheme [54]. To determine a suitable k-point set, we performed geometry optimization for CO_2 adsorbed on the (2 × 2) CaO (1 0 0) surface from gamma point (denoted by 1 × 1) to (4 × 4 × 1) k-point (denoted by 4 × 4). Subsequently, we calculated the CO_2 adsorption energy as a function of the k-point set. As shown in Fig. S2, the effect of k-point sampling on the adsorption energy is diminished beyond the (2 × 2) k-point in both cases. Therefore, (2 × 2) k-point sampling was used to study all the characteristics of the CO_2-CaO system.

3. Results and discussion

3.1. Synthesis of porous bimodal Ca-based materials

Changes in morphology can promote the activation of additional adsorption sites for CO_2. In the present study, we attempted to control the architecture of porous Ca-based materials by changing the drying method (OD, FD, AD, and FAD). Representative TEM images shown in Fig. 1 reveal the morphology and structure of various porous Ca-based materials. From a structural point of view, the drying method influences the phase of the material, resulting in the formation of various structures from simple cubic (SC) to truncated simple cubic (TSC). When FD or AD process is applied as the drying method, truncation takes place to carve polytope vertices in any dimension, which exposes new facet sites in the place of vertices. In terms of geometry, the developed porous material is in the form of distinct irregular and polyhedral polycrystalline particles in linking ingrown groups after non-uniformed truncation, which refers to an intermediate between cubic and cubo-octahedral structure. The exposed truncated regions can act as

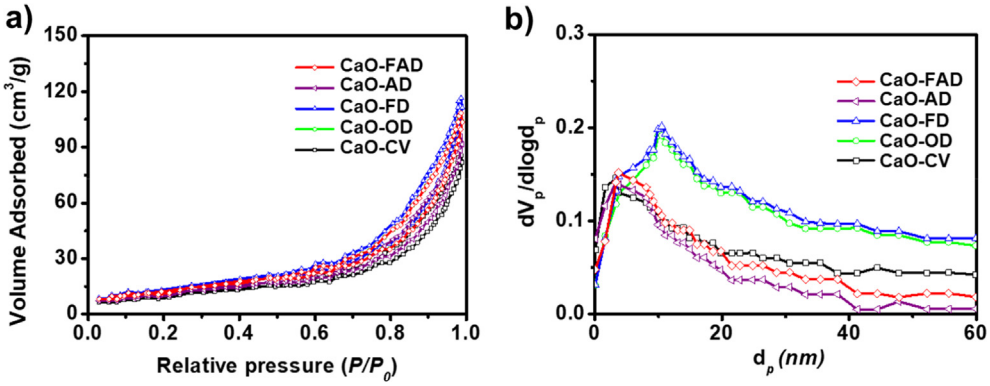

Fig. 2. (a) N_2 adsorption–desorption isotherms and (b) pore size distributions of porous bimodal Ca-based materials.

additional adsorption sites for CO_2. Aerogel drying induces more truncation in each vertex of the sample. After using aerogel drying process for 1 h, supercritical CO_2 dramatically expands the pores and truncates the precipitated crystal structure, which leads to the formation of the unstable Ca-based materials surface and phase transformation of the structure (See supplementary information: Fig. S3). However, the AD process for 3 h duration may be able to give a stability of the exposed pore surface of the adsorbent, resulting in the formation of various Ca-based materials such as CaO, $Ca(OH)_2$ and $CaCO_3$.

To characterize the textural properties of various adsorbents, we performed nitrogen adsorption–desorption isotherm analysis, as shown in Fig. 2(a). For all samples, the small amount of adsorption volume indicates the IV-type isotherm with H1-type hysteresis loop, owing to the formation of truncation-shaped agglomerates or compacts. This can be attributed either by the partial blocking of the porous network by truncated mixture crystalline of CaO and $Ca(OH)_2$ or by structural transformation into the truncated phase. Fig. 2(b) also shows the BJH pore size distribution of the adsorbents and Table 1 summarized the textural properties of adsorbents. CaO-OD and CaO-FD exhibited relatively large pore size distribution, but total pore volume and BET surface area were not shown quite different. It is noteworthy that the truncated phase is more predominant characteristics for indicative textural properties to improve adsorption capacity. In terms of physical properties of the synthesized adsorbents, precipitation synthesis using FD does not result in a significantly different pore structure as that using oven drying, whereas AD process reduced the BET surface area, pore size and pore volume of samples compared to those with OD process, owing to the additional calcination process at 900 °C that was performed to remove the carbonation species formed by CO_2 exposed on the CaO surface during aerogel drying (Table 1). Interestingly, even after calcination process at high temperature, CaO-FAD shows stable morphology and structure in accordance with high CO_2 capacity, which confirms the important role of freezing drying on the pore creation and aerogel drying on the activation of the surface, simultaneously.

Table 1
Physical properties of various CaO adsorbents.

Sample	BET surface area (m^2/g)[a]	Pore size (nm)[b]	Pore volume (cm^3/g)[b]	Particle size (CaO/Ca(OH)$_2$ (nm)[c]	CO_2 Chemisorption (wt.%)		
					Total	Partial @ < 400 °-C	Partial @ > 400 °-C
CaO-CV	22.4	1.64	0.14	n.a	3.45	1.04	2.41
CaO-OD	50.1	10.55	0.16	26.6/5.9	7.32	2.54	4.78
CaO-FD	51.0	10.50	0.19	26.0/6.6	8.38	3.22	5.16
CaO-AD	43.5	3.3	0.11	47.7/10.3	5.54	2.43	3.12
CaO-FAD	40.8	3.72	0.16	54.7/10.0	14.81	5.08	9.73

[a] Surface area was calculated by BET method.
[b] Pore size and pore volume was calculated by BJH method with mesoporous range of 2–50 nm.
[c] Particle size was calculated by Scherrer formula.

To elucidate the structure of the adsorbents, we carried out XRD analysis to determine the crystallinity of the porous structures as a function of various drying methods. As shown in Fig. 3, The XRD patterns show the native cubic CaO structure in all samples, whereas the $Ca(OH)_2$ peaks are generated according to the drying conditions of the present study. It is noted that although some XRD patterns are superimposed for the CaO and $Ca(OH)_2$, most of the typical patterns are closely spaced but well-distinguished. We were able to calculate the particle sizes at XRD peaks and are shown in Table 1. The relationship between particle size and CO_2 adsorption performance is not clear, but is believed to result in an increase in CO_2 adsorption due to the combination of increased particle size and surface properties through combined drying processes (FAD).

During the synthesis process, $Ca(OH)_2$ undergoes dehydration reaction of OH^- species to form CaO. However, when NaOH solution is added, sufficient OH^- is available to recover $Ca(OH)_2$ in the drying process to form a dual phase structure of CaO and $Ca(OH)_2$. Lin et al. [36] found that the CO_2 adsorption capacity of $Ca(OH)_2$ is better than that of commercial CaO, which suggests that the presence of residual Ca$(OH)_2$ enhances the adsorption performance. From XRD patterns, clear bi-modal crystal structure shows the high intensity of CaO rather than $Ca(OH)_2$. It suggests that the slow dehydration reaction still hindered

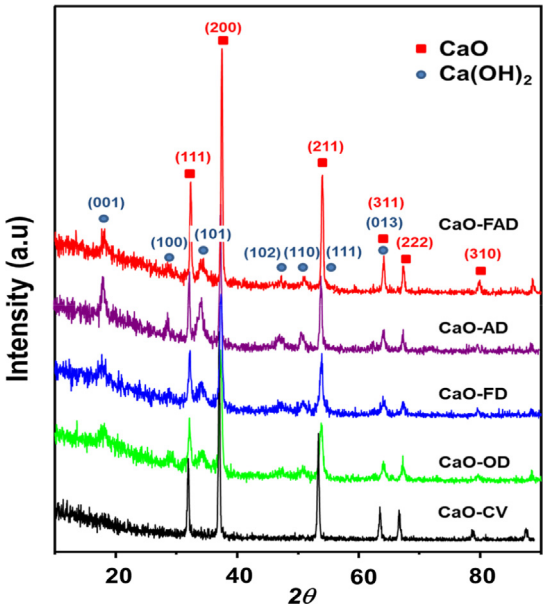

Fig. 3. XRD patterns of porous bimodal Ca-based materials.

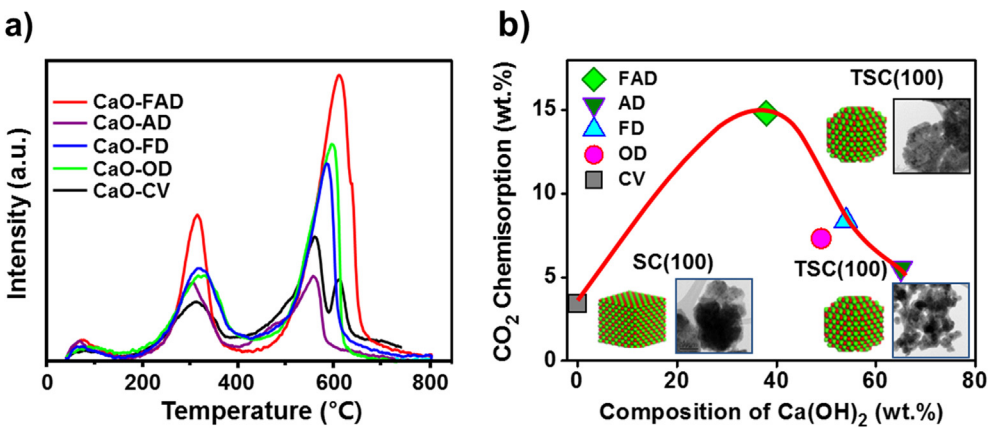

Fig. 4. Chemisorption capacity of various porous bimodal CaO-based adsorbents using CO_2-temperature programmed desorption (TPD) experiments: (a) TPD profile as a function of temperature, (b) Trends in CO_2 chemisorption capacities with respect to the contents of $Ca(OH)_2$ with the proposed crystal phase and TEM images of samples. SC, TSC refer to simple cubic, truncated simple cubic, respectively.

full CaO formation, which remains $Ca(OH)_2$ phase. It was expected that bimodal-type adsorption mechanism is operated with CO_2 as shown in Eqs. (1) and (2). In addition, the (2 0 0) facet of the CaO in all the samples is predominantly exposed to the reaction, followed by the (1 1 1) and (2 1 1) facets, in that order.

3.2. CO_2 adsorption capacity on porous architectures

3.2.1. Static CO_2 adsorption profile

To elucidate the correlation between the CO_2 adsorption capacity and structure of various bimodal Ca-based materials, we measured the CO_2 temperature programmed desorption (TPD) profiles for the capability of chemisorption. Fig. 4a and Table 1 show that in general, two peaks are observed, one at low (~350 °C) and the other at high temperatures (570–620 °C).

The chemisorption capacities of CaO-AD are dramatically reduced, although the CO_2 adsorption capacities of the CaO-AD samples are higher than that of conventional CaO. It is found that AD method itself causes sintering of the particles during the removal of the carbonation species produced during the drying process. As a result, the size and volume of the pores are reduced, and also the active adsorption sites decreased, resulting in a decrease in adsorption capacity, as shown in Table 1. Interestingly, however, samples synthesized by the combination of FD and AD drying processes (FAD) exhibit the highest peak intensity corresponding to a high degree of chemisorption (> 14.8 wt %) in the measured temperature range, suggesting that the surface of CaO-FAD significantly enhances the affinity to CO_2 molecules by 4 times compared to conventional CaO, which is attributed to the increase in the basicity of the surface. Exposure of more active sites on the basic surface in the truncated structure can increase the basicity of the surface, leading to a more favorable surface reaction. Therefore, although the size and volume of the pores at the samples are reduced after calcination, the combined drying process (FAD) could optimize pore and surface properties for CO_2 adsorption. In addition, Fig. 4b shows the correlation of the CO_2 chemisorption capacities according to $Ca(OH)_2$ contents in the CaO-based bimodal structure. The content of $Ca(OH)_2$ was calculated by quantitative analysis determining the relative factor through integrated intensity of the XRD peaks of CaO and $Ca(OH)_2$ with the Rietveld refinement. It is noted that the content of $Ca(OH)_2$ is defined as weight percent (wt.%). From the asymmetrical "volcano-type" relation of the capacities of chemisorbed CO_2 with respect to their $Ca(OH)_2$ contents, it can be inferred that the amount of $Ca(OH)_2$ could act as an important descriptor for the adsorption properties and performances, such as adsorption capacity, adsorptive energy, and the charge transfer amount during the adsorption process. Interestingly, in the single drying process such as FD, AD and OD, the content of $Ca(OH)_2$ was high, whereas the combined FAD process exhibited the maximum CO_2 adsorption capacity by controlling the $Ca(OH)_2$ content. As the content of $Ca(OH)_2$ increases at an early stage to 38 wt%, the chemisorption capacity remarkably increases from 3.45 to 14.8 wt%, resulting from the beneficial role of bimodal structure. When the $Ca(OH)_2$/CaO content ratio reaches above 40 wt%, the CO_2 adsorption capacity dramatically decreases to about 5.5 wt%. From the point of morphological view, the adjusted $Ca(OH)_2$ content increased accessible surface adsorption site to lead high CO_2 adsorption capacity, but the high content of $Ca(OH)_2$ over bimodal Ca-based materials limits the adsorptive performance since the passivation of the exposed pore surface of the adsorbent prevents interactions between the introduced CO_2 and the adsorbent surface. For the high contents of $Ca(OH)_2$ in mixture crystalline, the formation of truncation-shaped agglomerates or compacts causes either the partial blocking of the porous network or structural transformation into the truncated phase, which inhibits the adsorptive performance. Also, from a structural point of view, the single drying process (FD, AD and OD) developed mostly high $Ca(OH)_2$ contents because they limit the dehydration reaction of OH^- to form CaO. These results support that the controlled content of $Ca(OH)_2$ maintains a high porous structure, providing more adsorption sites, and CaO can adsorb more CO_2 chemically, which means CaO contents in the bimodal structure can play an important role on the adsorptive capacity. Finally, a series of sequential drying process (FAD) controlled $Ca(OH)_2$ content in CaO-based materials, which resulting in optimized the properties of the adsorptive surface and enhanced the CO_2 chemisorption performances.

3.2.2. Dynamic CO_2 adsorption profile

A similar correlation is found between the structural shape and flow dynamic CO_2 capture. We performed flow dynamic experiments for determining CO_2 mineralization on various porous CaO samples in the temperature range of 450–650 °C at a gas composition of 15 vol% CO_2 in N_2 at 200 mL/min, as shown in Fig. 5. Under these experimental conditions, the adsorption capacities of all the samples increase with temperature. The CO_2 adsorption capacities of the porous CaO samples are higher than that of conventional CaO. In particular, the adsorption behavior of CaO-FAD reveals that the adsorbent reacts reasonably fast with CO_2 and shows remarkable CO_2 carbonation (up to 26.1 wt% at 650 °C), which is consistent with the results of the CO_2-TPD experiments. Such superior performance of the porous CaO samples is attributed to (1) high availability of active adsorption sites in terms of textual properties and (2) strong CO_2 binding energy driven by charge transfer, leading to facile access of the CO_2 molecules to the adsorbent surface for CO_2 carbonation at the molecular level.

Subsequently, these results support the major premise that the truncated porous CaO structure leads to improved adsorption performance because of more available sites. Since the adsorbed CO_2 molecules are linked to the CaO surface by valence bonds during adsorption process, they will usually occupy existing adsorption sites on the surface and multi-layer of chemisorbed molecules is formed to develop carbonate species. Thus, CaO-FAD that has optimized the properties of

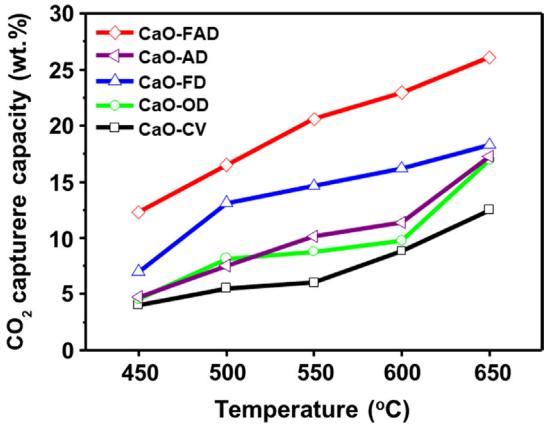

Fig. 5. Dynamic flow CO_2 adsorption on various adsorbents as a function of temperature. (Feed composition: 15 vol% CO_2 balanced with N_2, weight of adsorbent: 0.10 g, feed flow rate: 200 mL/min).

the adsorptive surface controlled by Ca-based materials can generate large amount of adsorption site for CO_2 capture.

Another series of multi-cycle tests (50 cycles of carbonation and de-carbonation) was further conducted using flue gas composed of 15% CO_2 in N_2 to determine the regeneration ability of the adsorbents. The used adsorbent was completely regenerated at a high temperature (800 °C) to recover its adsorption capacity and the results are shown in Fig. 6a.

The results obviously suggest that while adsorption becomes less stable with increase in the number of cycles, porous Ca-based adsorbents exhibit stable CO_2 adsorption capacity and good structural stability during the full regeneration cycle compared to conventional CaO.

These results further suggest that the carbonation kinetics depends on the composition of the adsorbent as well as the operating conditions in the reaction temperature range. During the cyclic carbonation performance, internal gas diffusion is gradually inhibited once a compact carbonate layer is generated on the adsorbent surface [37,38]. The CaO-CV adsorbent typically exhibits such diffusional inhibition, which ultimately terminates the carbonation reaction shortly. However, various bimodal Ca-based materials represent the stable cyclic adsorption capacity. In particular, CaO-FAD shows a relatively small drop in adsorption activity (less than 13%), clearly indicating that CaO-FAD could be utilized for the adsorption of CO_2 gas emitted from power plants.

To figure out the feasibility of the desired materials for CO_2 capture, we additionally performed another series of multi-cycle tests (50 cycles of carbonation and de-carbonation) using simulated flue gas mixtures of 15% CO_2 with air environment (17.7% O_2 with 67.3% N_2) in the same manner (Fig. 6b). The long term stability and the adsorption capacity of the adsorbents in oxygen presenting environment were still retained in all the successive cycles compared to those in nitrogen environment. In particular, the adsorption capacity of CaO-FAD remained the high binding efficiency corresponding to over 21 wt% up to 50 cycles because the truncated structures could reserve a chemically intact surface state with diminishing structural damage during multi-cyclic adsorption/regeneration operations, which leads to the facile regeneration of adsorbents. In contrast, adsorptive performance of others was gradually reduced as the number of cycles increased because the adsorbed CO_2 has a high tendency to aggregate and form non-uniformly distributed carbonates on the adsorbent surface, owing to the unstable surface phase. For CaO-AD in air condition, cyclic performance was significantly decreased compared to that in N_2 condition because remained supercritical CO_2 phase in the adsorbent matrix can readily react with O_2 to form carbonate phase on the surface so that the active surface for introducing CO_2 gas was diminished. It should be noted that the freezing drying with aerogel drying method leads to form a stable structure for adsorptive performance even in the air environment.

3.3. DFT calculations of single CO_2 molecule adsorption on CaO (1 0 0)

In addition to the CO_2 adsorption experiments, we also attempted to investigate the adsorption characteristics of the prepared adsorbent, in order to determine the adsorption mechanism, with particular focus on the binding nature of CO_2 adsorption at the molecular level. Since the experimental findings suggest that only a controlled content of $Ca(OH)_2$ preserves the porous morphology and enhance the chemisorption capacity, we mainly focused on CaO contents as the bimodal structure, which can play a main role on CO_2 adsorption capacity for theoretical calculation. In particular, the (2 0 0) facet is mainly exposed in the truncated CaO structure confirmed by XRD patterns. Thus, we focused on investigating the CO_2 adsorption mechanism on the surface of CaO (1 0 0).

3.3.1. Adsorption energy and geometry

First, in order to investigate the nature of CO_2 adsorption on the CaO (1 0 0) surface, we performed geometry optimization of the CO_2-CaO (1 0 0) surface. As summarized in Table 2, it is found that the calculated adsorption energy and geometry are in good agreement with the experimental results as well as other computational results (Table 2) [23,29].

This validates our calculations. As evident from Fig. 7, the geometry of CO_2 is significantly changed before and after the adsorption described via the geometry optimization. Specifically, the O_{CO2}-C_{CO2}-O_{CO2} bond angle is significantly reduced from 180° to 134.1° and 129.4° on

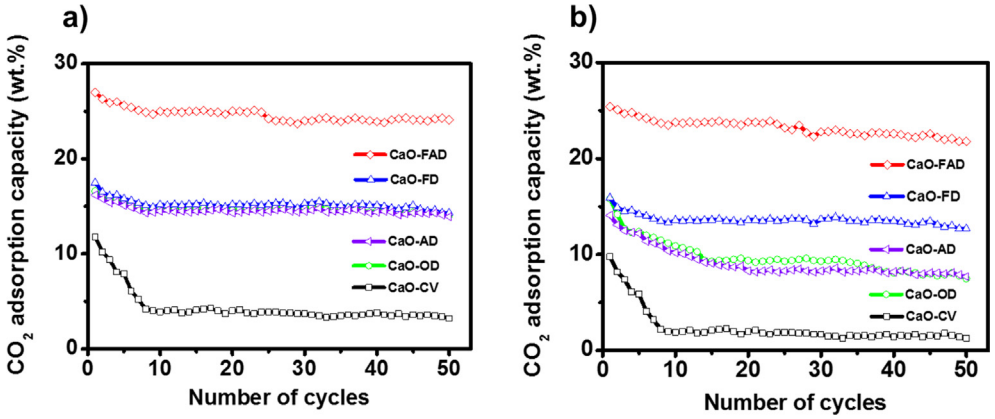

Fig. 6. Cyclic CO_2 adsorption capacity of the prepared adsorbents with the flue gas mixture of 15% CO_2 balanced with (a) N_2 and (b) with air (17.7% O_2 with 67.3% N_2) Note that carbonation was conducted at 650 °C and de-carbonation at 800 °C in 100% N_2 for 50 cycles of carbonation/de-carbonation.

Table 2
Geometries and energies for single CO_2 adsorption on CaO(1 0 0) surface.

	Bond length ($C_{CO_2} - O_{CaO}$) (Å)	Bond length ($C_{CO_2} - O_{CO_2}$) (Å)	Bond angle ($O_{CO_2} - C_{CO_2} - O_{CO_2}$) (degree)	Adsorption energy (eV)
Experiment [I] [29]				−1.1
Theory[II] [23]	1.38	1.23	130.0	−1.0
This study[III]	1.47	1.25	134.1	−0.94
This study[IV]	1.39	1.27	129.4	−1.76

[I] Adsorption energy obtained by the thermal desorption method.
[II] Ab-initio Hartree-Fock calculation.
[III] CO_2 adsorption on the (1 × 1) CaO surface.
[IV] CO_2 adsorption on the (2 × 2) CaO surface.

the (1 × 1) and (2 × 2) CaO surfaces, respectively, whereas the C_{CO2}-O_{CO2} bond length is increased from 1.18 Å to 1.25 Å and 1.27 Å for the (1 × 1) and (2 × 2) CaO surfaces, respectively. This indicates that the hybridization of the C_{CO2}-O_{CO2} bonds is changed from *sp* to sp_2 owing to the formation of a new chemical bond between the carbon atom of CO_2 and the oxygen atom on the CaO surface (C_{CO2}-O_{CO2}). The calculated adsorption energies (− 0.94 eV and − 1.56 eV for (1 × 1) and (2 × 2) CaO surface, respectively) are also consistent with new chemical bond formation. Thus, it is concluded that the CO_2 adsorption on the CaO (1 0 0) surface is a chemisorption process.

3.3.2. Charge reorganization

Pacchioni and coworkers suggested that such strong adsorption can be understood by considering the low Madelung potential energy of CaO due to the large cation-anion distance in the CaO matrix (2.405 Å) compared to the MgO matrix (2.118 Å). This leads to high basicity, which allows active donation of charge from the surface to the adsorbed molecule [23,24].

In this study, in order to evaluate such charge transfer, we calculated the charge difference for each atom: $\Delta q_{i,CaO}$ and $\Delta q_{i,CO_2}$ of CaO surface and CO_2, respectively, before and after the adsorption using Eqs. (4) and (5).

$$\Delta q_{i,CaO} = \Delta q_{i,CaO\ before\ adsorption} - \Delta q_{i,CaO\ after\ adsorption} \quad (4)$$

$$\Delta q_{i,CO_2} = \Delta q_{i,CO_2\ before\ adsorption} - \Delta q_{i,CO_2\ after\ adsorption} \quad (5)$$

where $\Delta q_{i,CaO\ before\ adsorption}$ and $\Delta q_{i,CaO\ after\ adsorption}$ denote the Mulliken charges of the i^{th} atom on the CaO surface before and after adsorption, respectively, and $\Delta q_{i,CO_2\ before\ adsorption}$ and $\Delta q_{i,CO_2\ after\ adsorption}$ denote the charges on the i^{th} atom of CO_2 before and after adsorption, respectively. Fig. 8 visualizes the charge reorganization on the CaO surface and CO_2 via charge transfer between them. Δq_i will have a negative value (blue color) if the i^{th} atom loses charges, whereas it will have a positive value (red color) if the atom gains charges. Therefore, it is clear that a charge of –0.7e is transferred from the CaO surface to the CO_2 molecule, as calculated from the Mulliken population analysis.

3.3.3. Effect of surface coverage

Single molecule adsorption of CO_2 on CaO (1 0 0) surfaces with various cell sizes such as the (1 × 1), (2 × 2), (3 × 3), and (4 × 4) supercells (corresponding to surface coverages (θ) of 0.5, 0.125, 0.055, and 0.032, respectively) was simulated via geometry optimization to investigate the effect of interactions between neighboring CO_2 molecules on the adsorption energy. At θ = 1.0, every oxygen atom on the CaO (1 0 0) surface is occupied by an adsorbed CO_2 molecule, whereas at θ = 0.0, no CO_2 is adsorbed on the CaO surface. As clearly shown in Fig. S4, the adsorption energy depends on the surface coverage of CO_2, indicating that the adsorbed CO_2 is influenced by neighboring adsorbed CO_2 molecules. Furthermore, it should be noted that the adsorption energy profile shows a minimum at a specific surface coverage, θ = 0.125 for the (2 × 2) supercell, where the electrostatic interactions between adsorbed CO_2 molecules stabilizes the adsorption. It appears that the adsorbed molecules may not undergo such electrostatic interactions at low coverage and thus, the adsorption becomes stronger slightly. On the other hand, at high coverage, the adsorbed molecules come too close to each other and therefore, electrostatic repulsion destabilizes the adsorption. The effect of surface coverage will be discussed further in the next section.

3.3.4. Proposed energy profile of CO_2 adsorption on CaO

To gain insights into the carbonation mechanism on the adsorbent surface, we calculated the energy change as a function of reaction coordinates. Fig. 9 presents the energetically favorable reaction profile. Initially, the CO_2 molecule is loaded at a distance of 3.0 Å from the CaO surface. From Fig. 8, it is observed that the interaction of CO_2 with CaO surface is not so sensitive to the CO_2-CaO surface distance down to a distance of 2.3 Å. Subsequently, CO_2 is readily adsorbed on the CaO surface with CO_2 hybridization.

3.4. DFT calculations of the adsorption of multiple CO_2 molecules

3.4.1. Formation of a monolayer

Although multiple CO_2 molecules can be adsorbed on CaO (1 0 0) surfaces, such simulation studies have not been performed or reported

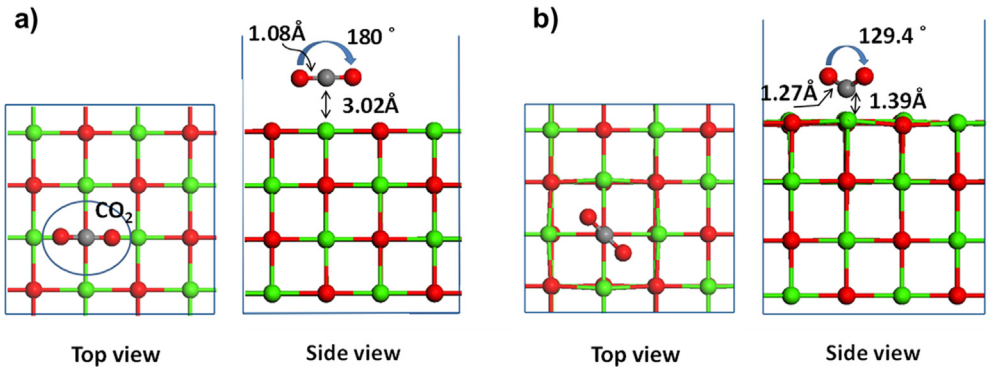

Fig. 7. Geometries of a single CO_2 molecule adsorbed on a (2 × 2) CaO (1 0 0) surface (a) before geometry optimization and (b) after geometry optimization. Bond length between the carbon and oxygen atom in the CO_2 molecule, inter-atomic distance between the carbon atom in CO_2 and oxygen atom on the CaO surface. The angles are shown in the side views. The optimized structure shows an elongated bond length of 1.27 Å, decreased angle of 129.4°, and inter-atomic distance of 1.39 Å, consistent with chemisorbed CO_2. The green, red, and gray balls denote calcium, oxygen, and carbon atoms, respectively, whereas the outer solid lines indicate periodic cell boundaries.

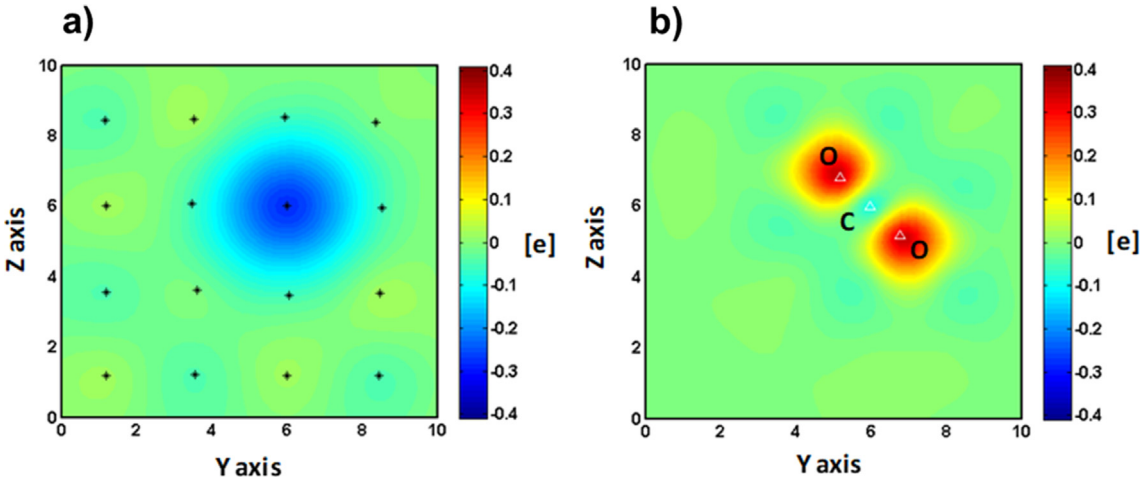

Fig. 8. Charge reorganization on the (a) CaO (1 0 0) surface and (b) CO_2 molecule. Note that a positive value (red color) implies electron gain after CO_2 adsorption, whereas a negative value (blue color) implies electron loss compared to the original charges on the CaO surface and CO_2 molecule (For interpretation of the references to colour in this figure legend, the reader is referred to the web version of this article.)

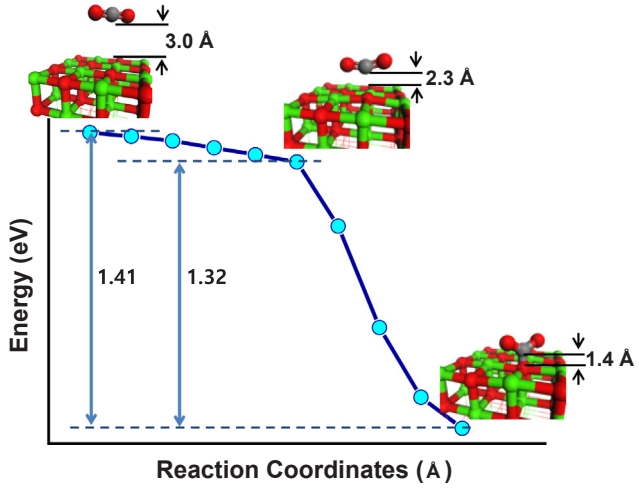

Fig. 9. Energy profile associated with CO_2 adsorption on CaO (1 0 0) calculated using DFT calculation. The energy barrier for CO_2 adsorption on the CaO surface to form $CaCO_3$ is also shown.

yet to the best of our knowledge. In the present study, the formation of the multiple CO_2 monolayer was simulated using DFT in order to understand how the CO_2 molecules affect each other when they are adsorbed on the CaO (1 0 0) surface (Fig. 10). In the study on the adsorption of a single CO_2 molecule discussed in the previous section, we already observed that the adsorption energy is affected by surface coverage, and the most stable surface coverage is ~0.125 (Fig. S4).

Here, the surface coverage is scrutinized in-depth for the case of the adsorption of multiple CO_2 molecules. In order to determine the most stable surface coverage, various systems consisting of multiple CO_2 molecules were built (Table S1). The geometries of the systems were then optimized. For example, since the (1 × 1) CaO (1 0 0) surface has two oxygen atoms (Fig. S1b), we can place CO_2 molecule on one of the two oxygen atoms or two CO_2 molecules on both two oxygen atoms. Fig. S5, which shows the optimized geometries for these two cases, reveals that the (1 × 1) CaO (1 0 0) surface can accommodate only one CO_2 molecule. Although two CO_2 molecules are attached on the oxygen atoms at the beginning, only one CO_2 molecule can undergo chemisorption with an oxygen atom, while the other CO_2 molecule moves away from the surface. In the case of the (2 × 2) CaO (1 0 0) surface, we attached up to eight CO_2 molecules and performed geometry optimization. However, as shown in Fig. 9a, only four CO_2 molecules are chemisorbed non-uniformly on the CaO surface, whereas the rest of the molecules are detached. Any attempt to place more than four CO_2 molecules fails. Thus, it is inferred that the maximum surface coverage is $\theta = 0.5$.

Further, the adsorption energy was calculated as a function of surface coverage using the (2 × 2) CaO (1 0 0) surface with multiple CO_2

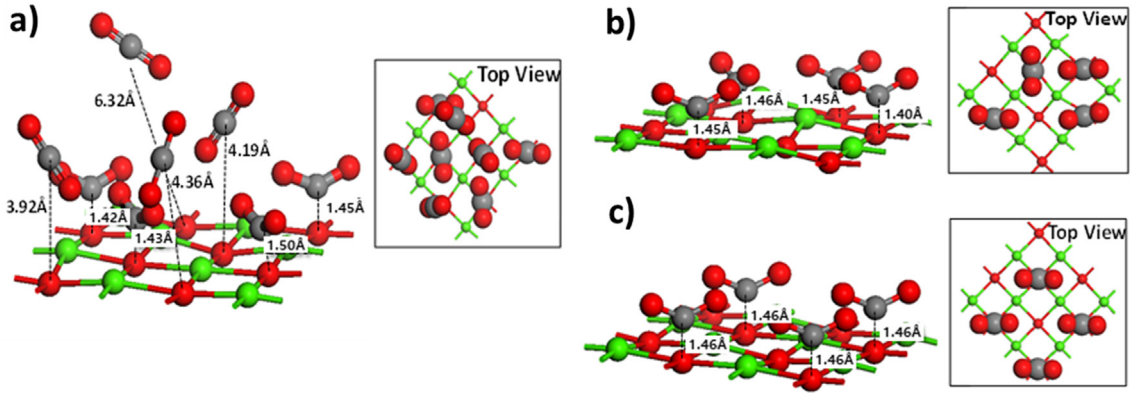

Fig. 10. Optimized geometry of the eight CO_2 molecules on the (2 × 2) CaO (1 0 0) surface. Each figure shows CO_2 molecules on the first layer of the (2 × 2) CaO surface. (a) full adsorption; (b) non-uniform adsorption on the sites. Here, four CO_2 molecules are adsorbed when eight CO_2 molecules are loaded on the surface; (c) uniform adsorption. The green, red, and gray balls denote calcium, oxygen, and carbon atoms, respectively.

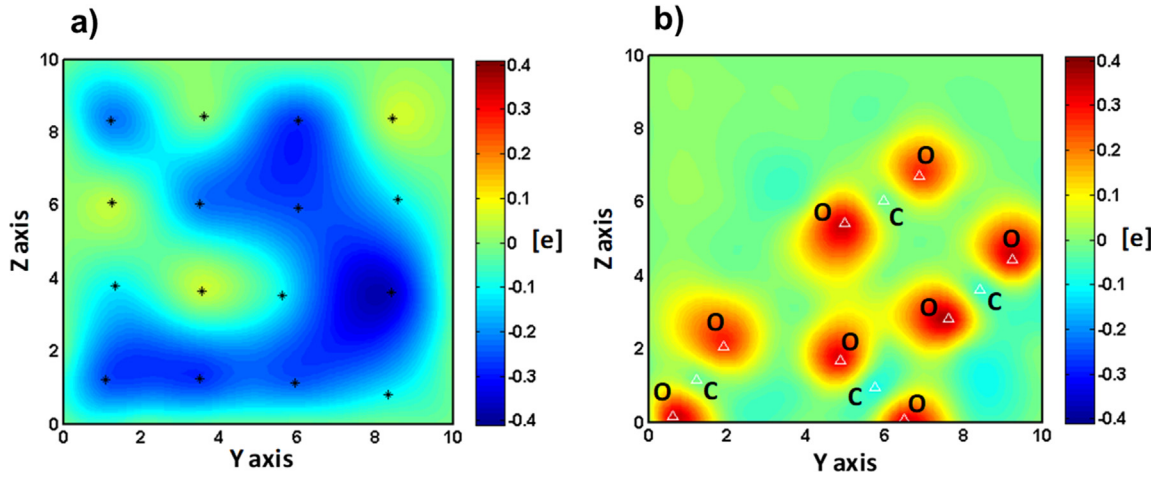

Fig. 11. Charge reorganization on the (a) CaO (1 0 0) surface and (b) four CO_2 molecules. Note that a positive value (red color) implies electron gain after CO_2 adsorption, whereas a negative value (blue color) implies electron loss compared to the original CaO surface and CO_2 molecule. (For interpretation of the references to colour in this figure legend, the reader is referred to the web version of this article.)

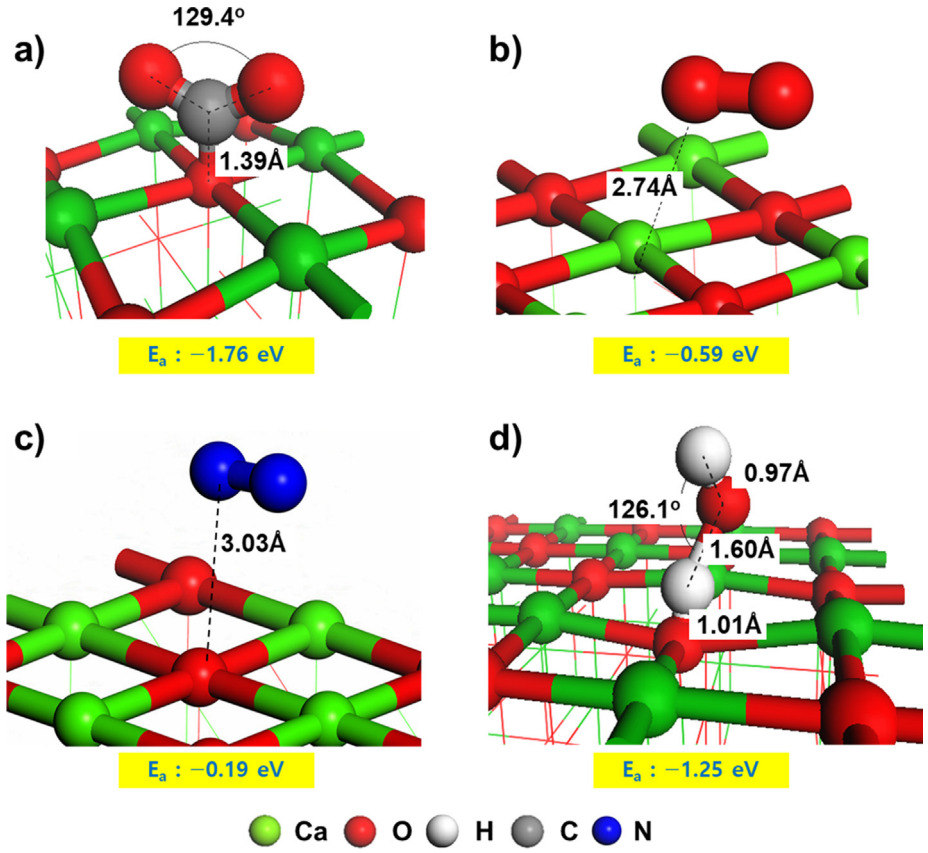

Fig. 12. Single gas adsorption of (a) CO_2, (b) O_2, (c) N_2, (d) H_2O on the CaO (1 0 0) surface.

molecules. From Table S1, it is confirmed again that the adsorption becomes weaker with increasing number of molecules. Thus, from our study, the most stable surface coverage is found at θ = 0.125, corresponding to 92.56 $Å^2/CO_2$ molecule, which is consistent with the formation of the CO_2 monolayer.

3.4.2. Charge reorganization

In the previous section, we suggested that charge reorganization occurs on the CaO surface owing to charge transfer from the CaO surface to the CO_2 molecule. We suppose that this charge reorganization is crucial in determining the most stable surface coverage of CO_2 since the atomic charges of CO_2 on CaO surface will repel other CO_2 molecules.

In Fig. 11, the charge reorganization of the CaO surface as well as the adsorbed CO_2 molecules are presented. As expected, the charges are transferred from the CaO surface to the CO_2 molecules, similar to the phenomenon observed in Fig. 8. The amount of charge transferred is –0.66e/CO_2 molecule, on average. However, it is worthwhile to note that the adsorbed CO_2 molecules are aggregated together rather than spread out uniformly over the CaO surface. This can be understood by considering that the CO_2 molecules experience inter-molecular electrostatic attraction between the negatively charged oxygen atoms (–0.58e on average) and the positively charged carbon atoms to some

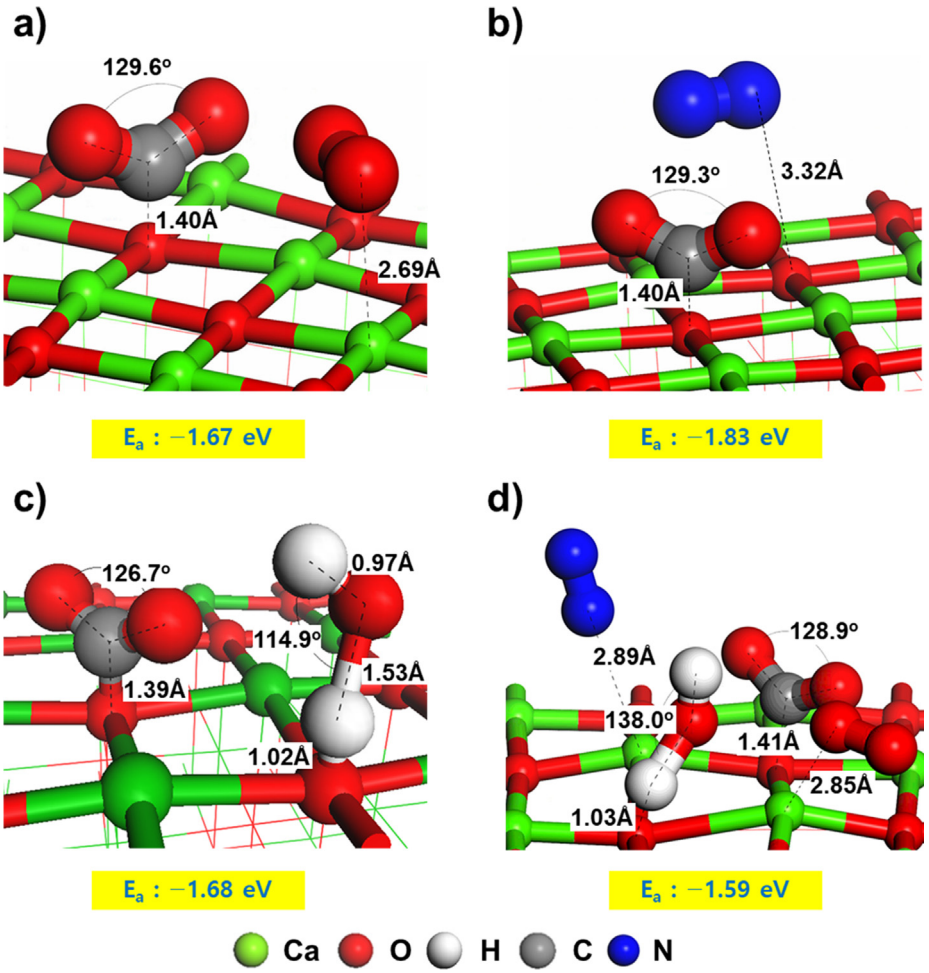

Fig. 13. Competitive adsorption of CO_2 with (a) O_2, (b) N_2, (c) H_2O, (d) various gas mixtures (i.e., O_2, N_2, and H_2O) on the CaO (1 0 0) surface.

extent since the adsorbed CO_2 molecules have positively charged carbon atoms (–0.56e on average). Therefore, there should be an optimal inter-molecular distance between CO_2 and CaO surface corresponding to stable adsorption, which is ~1.46 Å on average. Indeed, by simulating an independent system having uniform CO_2 adsorption, for comparison, it is found that the adsorption energy from non-uniform CO_2 adsorption (–1.08 eV from Fig. 10b) is significantly lower (meaning stronger adsorption) than that from uniform adsorption (–0.83 eV from Fig. 10c), implying that non-uniform adsorption is more stable than uniform adsorption.

3.5. DFT calculations of the competitive adsorption of gas mixtures

To identify the adsorption properties of real gas mixtures on CaO, we additionally investigated the adsorption geometry of various types of single gas molecule such as CO_2, N_2, O_2, H_2O, mainly composed of flue gas mixtures, as shown in Fig. 12. We quantitatively analyzed and compared the adsorption capacity for the optimized geometries for the adsorption of various gas types on the 2 × 2 CaO (1 0 0) surface.

The reduced bond lengths and high adsorption energy of optimized systems confirm a readable affinity of CO_2 and H_2O uptake on the CaO surface, but air composites (i.e., N_2, O_2) are just adsorbed moderately. In comparison of adsorption energies of various molecules, CO_2 (E_a = –1.76 eV) is energetically more preferable to CaO than other gases, owing to the stronger interaction of CO_2-CaO system, driven by more distributed charge transfer. These results provide the CaO surface has a resistance to the oxidative formation by air intake, corresponded by experimental results (Fig. 6b). In particular, the adsorption characteristics of H_2O molecule on CaO determine the adsorption affinity of water vapor in the flume gas mixtures (Fig. 12d). The optimized geometry provides a bond length of $O_{surface}$-HOH (1.01 Å), H-$OHO_{surface}$ (i.e., one short OH of single H_2O molecule) (0.97 Å), and HO-$HO_{surface}$ (i.e., elongated OH bond) (1.60 Å). This result clearly represents a partial dissociation of H_2O molecule to build a calcium hydroxide layer with surface sites because the surface of oxidic adsorbent matrix has a high tendency to readily saturate with H^+ and OH^- molecules, owing to the highly Lewis-basic and -acidic property of the oxygen sites and Ca^{2+} sites, respectively. This indicates that a net electron donation of CO_2 molecule is higher than that of H_2O molecule, which shows that CO_2 adsorption tends to take place rather than H_2O adsorption on the surface.

Concomitant with single gas adsorption characteristics, we determined the competitive adsorption of various gas mixtures to determine the adsorption characteristics of CO_2 and H_2O in the air environment on the CaO surface since the presence of water vapor in real flue gas mixtures remains the relevant issue for water vapor effect on CO_2 adsorption (Fig. 13). From the competitive adsorption of CO_2 and rest gas mixtures (i.e. N_2, O_2, and H_2O), CaO shows still high enough affinity of CO_2 to the oxygen site with high adsorption energy (< –1.59 eV). Experiment results also support high resistance of the CaO surface to air environment. Under air environment, CO_2 and H_2O molecules are simultaneously adsorbed on the free oxygen sites of the CaO surface to form carbonate ($CaCO_3$) and calcium hydroxide ($Ca(OH)_2$), respectively, attributed to strong Lewis–basic and –acidic interaction between the oxygen sites of CaO, and carbon of CO_2 and hydrogen of H_2O. The interaction diminished the bond strength of O–C

for CO_2 and O–H for H_2O, which leads the bending of CO_2 molecule and elongating H–OH bond of H_2O due to the readable hybridization. Nevertheless, competitive adsorption of CO_2 and other components barely affect CO_2 uptake on CaO. The electrostatic stabilization of CO_2 referred to the high adsorptive capacity of CO_2, provided by the strong electron interaction. It is worthy to note that CO_2 are chemisorbed on the CaO surface under various gas mixtures.

4. Conclusions

We introduced porous architecture in bimodal calcium-based materials by adopting various drying processes during synthesis in order to enhance the physical properties of the adsorbents and activate additional adsorption sites. We suggest that the various drying methods on porous structure develop different composition ratio of CaO and Ca$(OH)_2$ in bimodal materials, and in particular, formation of different morphology and structure, which leads different adsorption characteristics. On the basis of these findings, we observed the synergic effect of CaO and Ca$(OH)_2$ composites on CO_2 adsorption. In particular, this study proposes that the truncated porous structure prepared by applying FD and AD methods in combination plays an important role in enhancing CO_2 adsorption on calcium-based materials. This finding results from the opening of active adsorption sites and high CO_2 adsorptive binding energy. Both static and dynamic adsorption experiments support the finding that CO_2 adsorption is strongly improved on truncated calcium-based materials. Since to be equivalent to the capacity of CO_2 mineralization, the price of bimodal porous Ca-based materials is approximately 3 times cheaper than that of conventional CaO, we believe more research can reduce the expense of synthesis significantly after the optimized synthesis procedure, which can be suitable on the cost-effective adsorbents for feasible application. In addition, this study examines the adsorption of multiple CO_2 molecules on a CaO (1 0 0) surface using DFT calculation to understand its mechanisms and characteristics. It is clear that CO_2 adsorption is a chemisorption process that occurs via charge transfer from the CaO surface to CO_2 molecule, leading to monolayer formation on the adsorbent surface. The adsorbed CO_2 molecules tend to be aggregated rather than be distributed uniformly over the CaO surface. However, the adsorption is destabilized with increase in the number of CO_2 molecules. We expect that this study would extend understanding of the adsorption mechanism of CO_2 molecules on CaO and provide a basis for studying CO_2 adsorption on natural calcium-based minerals such as wollastonite ($CaSiO_3$) and diopside ($CaMgSi_2O_6$).

Declaration of Competing Interest

The authors declare no competing financial and non-financial interest.

Acknowledgements

This work was supported by funds from Samsung Electronics Co. Ltd. A relevant patent application is in progress by Samsung Electronics Co. Ltd. This work was supported by the National Research Foundation of Korea (NRF) grant funded by the Korea government (MSIT) (No. NRF-2019R1A2C2008733).

Appendix A. Supplementary material

Supplementary data to this article can be found online at https://doi.org/10.1016/j.apsusc.2019.144512.

References

[1] B. Metz, O. Davidson, H.D. Coninck, M. Loos, L. Meyer, IPCC Special Report on Carbon Dioxide Capture and Storage, Cambridge University Press, Cambridge, 2005.
[2] Inventory of U.S., Greenhouse Gas Emissions and Sinks: 1990–2006, Environmental Protection Agency, 2008.
[3] IEA, CO2 emissions from fuel combustion, Internatinal Energy Agency (IEA) Statistics Data, 2009.
[4] J.C. Hicks, J.H. Drese, D.J. Fauth, M.L. Gray, G.G. Qi, C.W. Jones, Designing adsorbents for CO_2 capture from flue gas-hyperbranched aminosilicas capable, of capturing CO2 reversibly, J. Am. Chem. Soc. 130 (2008) 2902–2903.
[5] M.L. Gray, Y. Soong, K.J. Champagne, H. Pennline, J.P. Baltrus, R.W. Stevens, R. Khatri, S.S.C. Chuang, T. Filburn, Improved immobilized carbon dioxide capture sorbents, Fuel Process. Technol. 86 (2005) 1449–1455.
[6] D. Ko, R. Siriwardane, L.T. Biegler, Optimization of a pressure-swing adsorption process using zeolite 13X for CO_2 sequestration, Ind. Eng. Chem. Res. 42 (2003) 339–348.
[7] B.K. Na, K.K. Koo, H.M. Eum, H. Lee, H.K. Song, CO_2 recovery from flue gas by PSA process using activated carbon, Korean J. Chem. Eng. 18 (2001) 220–227.
[8] K. Miura, H. Nakagawa, H. Okamoto, Production of high density activated carbon fiber by a hot briquetting method, Carbon 38 (2000) 119–125.
[9] N.D. Hutson, S.A. Speakman, E.A. Payzant, Structural effects on the high temperature adsorption of CO_2 on a synthetic hydrotalcite, Chem. Mater. 16 (2004) 4135–4143.
[10] Z. Yong, V. Mata, A.E. Rodriguez, Adsorption of carbon dioxide onto hydrotalcite-like compounds (HTlcs) at high temperatures, Ind. Eng. Chem. Res. 40 (2001) 204–209.
[11] M.M. Maroto-Valer, D.J. Fauth, M.E. Kuchta, Y. Zhang, J.M. Andresen, Activation of magnesium rich minerals as carbonation feedstock materials for CO_2 sequestration, Fuel Process. Technol. 86 (2005) 1627–1645.
[12] A.R. Millward, O.M. Yaghi, Metal-organic frameworks with exceptionally high capacity for storage of carbon dioxide at room temperature, J. Am. Chem. Soc. 127 (2005) 17998–17999.
[13] E. Ochoa-Fernandez, M. Ronning, X.F. Yu, T. Grande, D. Chen, Compositional effects of nanocrystalline lithium zirconate on its CO_2 capture properties, Ind. Eng. Chem. Res. 47 (2008) 434–442.
[14] A. Meisen, X.S. Shuai, Research and development issues in CO_2 capture, Energy Convers. Manage. 38 (1997) S37–S42.
[15] R.A. Khatri, S.S.C. Chuang, Y. Soong, M. Gray, Carbon dioxide capture by diamine-grafted SBA-15: a combined Fourier transform infrared and mass spectrometry study, Ind. Eng. Chem. Res. 44 (2005) 3702–3708.
[16] R.A. Khatri, S.S.C. Chuang, Y. Soong, M. Gray, Thermal and chemical stability of regenerable solid amine sorbent for CO_2 capture, Energy Fuels 20 (2006) 1514–1520.
[17] M.G. Plaza, C. Pevida, A. Arenillas, F. Rubiera, J.J. Pis, CO_2 capture by adsorption with nitrogen enriched carbons, Fuel 86 (2007) 2204–2212.
[18] R.H. Niswander, D.J. Edwards, M.S. Dupart, J.P. Tse, A more energy-efficient product for carbon-dioxide separation, Sep. Sci. Technol. 28 (1993) 565–578.
[19] A. Veawab, P. Tontiwachwuthikul, A. Chakma, Corrosion behavior of carbon steel in the CO_2 absorption process using aqueous amine solutions, Ind. Eng. Chem. Res. 38 (1999) 3917–3924.
[20] P. Goldberg, Z.Y. Chen, W. O'Connor, R. Walters, H. Ziock, CO_2 mineral sequstration situation in US, J. Energy Environ. Res. 1 (1) (2001) 117.
[21] W. Seifritz, CO_2 disposal by means of silicates, Nature 345 (1990) 486.
[22] R.P. Walters, Z.Y. Chen, P. Goldberg, K. Lackner, M. McKelvy, H. Ziock, Mineral Carbonation: A Viable Method for CO_2 Sequestration, The National Energy Technology Laboratory, Morgantown, West Virginia, 1999.
[23] G. Pacchioni, J.M. Ricart, F. Illas, Ab-initio cluster model-calculations on the chemisorption of CO_2 and SO_2 probe molecules on MgO and CaO (100) surfaces – a theoretical measure of oxide basicity, J. Am. Chem. Soc. 116 (1994) 10152–10158.
[24] H.J. Freund, M.W. Roberts, Surface chemistry of carbon dioxide, Surf. Sci. Rep. 25 (1996) 225–273.
[25] S.F. Wu, T.H. Beum, J.I. Yang, J.N. Kim, Properties of Ca-base CO_2 sorbent using Ca(OH)(2) as precursor, Ind. Eng. Chem. Res. 46 (2007) 7896–7899.
[26] R.W. Hughes, D. Lu, E.J. Anthony, Y.H. Wu, Improved long-term conversion of limestone-derived sorbents for in situ capture of CO_2 in a fluidized bed combustor, Ind. Eng. Chem. Res. 43 (2004) 5529–5539.
[27] P. Sun, J.R. Grace, C.J. Lim, E.J. Anthony, Investigation of attempts to improve cyclic CO_2 capture by sorbent hydration and modification, Ind. Eng. Chem. Res. 47 (2008) 2024–2032.
[28] M.B. Jensen, L.G.M. Pettersson, O. Swang, U. Olsbye, CO_2 sorption on MgO and CaO surfaces: a comparative quantum chemical cluster study, J. Phys. Chem. B 109 (2005) 16774–16781.
[29] D. Cazorlaamoros, J.P. Joly, A. Linaressolano, A. Marcillagomis, C.S. Delecea, CO_2-CaO surface and bulk reactions – thermodynamic and kinetic approach, J. Phys. Chem. 95 (1991) 6611–6617.
[30] E.J. Karlsen, M.A. Nygren, L.G.M. Pettersson, Comparative study on structures and energetics of NOx, SOx, and COx adsorption on alkaline-earth-metal oxides, J. Phys. Chem. B 107 (2003) 7795–7802.
[31] J.M.C. Plane, R.J. Rollason, Kinetic study of the reactions of CaO with H_2O, CO2, O_2, and O_3: implications for calcium chemistry in the mesosphere, J. Phys. Chem. A 105 (2001) 7047–7056.
[32] M.A. Nygren, L.G.M. Pettersson, Theoretical modeling of metal-oxides – influence of field-strength on atomic oxygen-adsorption and a simple-model reaction – O-Ads + Co-]Co_2, Chem. Phys. Lett. 230 (1994) 456–462.
[33] S. Kwon, J. Hwang, H. Lee, W.R. Lee, Interactive CO_2 adsorption on the BaO (100) surface: a density functional theory (DFT) study, Bull. Korean Chem. Soc. 31 (2010) 2219–2222.
[34] M. Tutuianu, O.R. Inderwildi, W.G. Bessler, J. Warnatz, Competitive adsorption of

NO, NO_2, CO_2, and H_2O on BaO(100): a quantum chemical study, J. Phys. Chem. B 110 (2006) 17484–17492.
[35] H. Gronbeck, Mechanism for NO_2 charging on metal supported MgO, J. Phys. Chem. B 110 (2006) 11977–11981.
[36] J. Yu, X. Zeng, G. Zhang, J. Zhang, Y. Wang, G. Xu, Kinetics and mechanism of direct reaction between CO_2 and $Ca(OH)_2$ in micro fluidized bed, Environ. Sci. Technol. 47 (2013) 7514–7520.
[37] S.C. Kwon, M. Fan, H.F.M. Dacosta, A.G. Russell, C. Tsouris, Reaction kinetics of CO_2 carbonation with Mg-rich minerals, J. Phys. Chem. A 115 (2011) 7638–7644.
[38] S.C. Kwon, M.H. Fan, H.F.M. DaCosta, A.G. Russell, Factors affecting the direct mineralization of CO_2 with olivine, J. Environ. Sci. 23 (2011) 1233–1239.
[39] DMol3 module of Materials studio 2018, $DMol^3$ Module of Materials Studio 2018, Biovia, Inc, San Diego, 2018.
[40] Y.Y. Ahn, H. Bae, H.I. Kim, S.H. Kim, J.H. Kim, S.G. Lee, J. Lee, Surface-loaded metal nanoparticles for peroxymonosulfate activation: efficiency and mechanism reconnaissance, Appl. Catal. B-Environ. 241 (2019) 561–569.
[41] J.R. De Lile, S.G. Kang, Y.A. Son, S.G. Lee, Investigating polaron formation in anatase and brookite TiO2 by density functional theory with hybrid-functional and DFT plus U methods, ACS Omega 4 (2019) 8056–8064.
[42] Y.J. Kim, S.H. Kwon, H. Noh, S. Yuk, H. Lee, H.S. Jin, J. Lee, J.G. Zhang, S.G. Lee, H. Guim, H.T. Kim, Facet selectivity of Cu current collector for Li electrodeposition, Energy Storage Mater. 19 (2019) 154–162.
[43] J.H. Lee, S.H. Kwon, S. Kwon, M. Cho, K.H. Kim, T.H. Han, S.G. Lee, Tunable electronic properties of nitrogen and sulfur doped graphene: density functional theory approach, Nanomaterials-Basel 9 (2019).
[44] N.N.T. Pham, J.S. Park, H.T. Kim, H.J. Kim, Y.A. Son, S.G. Kang, S.G. Lee, Catalytic performance of graphene quantum dot supported manganese phthalocyanine for efficient oxygen reduction: density functional theory approach, New J. Chem. 43 (2019) 348–355.
[45] J.P. Perdew, K. Burke, M. Ernzerhof, Generalized gradient approximation made simple, Phys. Rev. Lett. 77 (1996) 3865–3868.
[46] J.P. Perdew, K. Burke, M. Ernzerhof, Local and gradient-corrected density functionals, Chem. Appl. Density-Funct. Theory 629 (1996) 453–462.
[47] P. Baranek, A. Lichanot, R. Orlando, R. Dovesi, Structural and vibrational properties of solid $Mg(OH)_2$ and $Ca(OH)_2$ – performances of various hamiltonians, Chem. Phys. Lett. 340 (2001) 362–369.
[48] P. Broqvist, I. Panas, E. Fridell, H. Persson, NO_x storage on BaO(100) surface from first principles: a two channel scenario, J. Phys. Chem. B 106 (2002) 137–145.
[49] M. Ernzerhof, J.P. Perdew, K. Burke, Density functionals: where do they come from, why do they work? Density Funct. Theory I (180) (1996) 1–30.
[50] H. Gronbeck, P. Broqvist, I. Panas, Fundamental aspects of NO_x adsorption on BaO, Surf. Sci. 600 (2006) 403–408.
[51] W. Koh, J.I. Choi, K. Donaher, S.G. Lee, S.S. Jang, Mechanism of Li adsorption on carbon nanotube-fullerene hybrid system: first-principles study, ACS Appl. Mater. Inter. 3 (2011) 1186–1194.
[52] W. Koh, J.I. Choi, S.G. Lee, W.R. Lee, S.S. Jang, First-principles study of Li adsorption on carbon nanotube (CNT) – Fullerene (C60) hybrid system, Carbon 49 (2011) 286–293.
[53] H.N. Waltenburg, P.J. Moller, Growth of ultrathin Cu films on CaO(100), Surf Sci. 439 (1999) 139–145.
[54] H.J. Monkhorst, J.D. Pack, Special points for Brillouin-zone integrations, Phys. Rev. B 13 (1976) 5188–5192.